Measurement Science and Technology, April 2006, Volume 17, Issue 4, pp605-616

Low-coherence optical fibre speckle interferometry

I Balboa[1], **H D Ford**[2, 3] **and R P Tatam**[2]
[1]PerkinElmer Optoelectronics, PerkinElmer Q-Arc Ltd, Saxon Way, Bar Hill, Cambridge CB3 8SL, UK.
[2]Optical Sensors Group, Centre for Photonics and Optical Engineering, School of Engineering, Cranfield University, Cranfield, Bedford, MK43 0AL, UK.

E-mail: h.d.ford@cranfield.ac.uk, R.P.Tatam@cranfield.ac.uk

Abstract. This paper describes the development of optical fibre low-coherence speckle interferometers capable of three-dimensional surface profiling with a resolution of 10-20 microns and a depth range of typically tens of centimetres. The technique is absolute, enabling the measurement of steps and through holes. The inclusion of optical fibres enables compact, flexible configurations to be realized, alleviating the experimental difficulties encountered with bulk interferometers, particularly when using long path lengths for measurements on large test objects. Sources including LEDs, SLDs and multimode laser diodes are compared, and the use of a multimode laser diode source in pulsed mode is shown to improve depth resolution.
Fibre-based systems using both single mode and polarization-maintaining fibre are described and the results of experimental measurements on a stepped test object, a tilted plate and a coin are presented. A depth resolution of ±20 μm is obtained for the standard fibre system, and ±14 μm for the system based on polarization-maintaining fibre.

Keywords: Low-coherence, speckle interferometry, profilometry, shape measurement
PACS Classification numbers: 42.10M, 42.30, 42.80

1. Introduction

Numerous techniques exist for determining the surface profile of an object [1]. The most basic methods use a stylus, placed in contact with the surface and tracked across it, to map out the shape [2]. These are point techniques, in which a single measurement acquires information from a single point on the surface. Since the stylus contacts the surface, there is a risk of measurement-induced damage; therefore non-contact, optical methods have been developed. Triangulation, which uses a light beam focused onto the surface, is the optical point-measurement equivalent of the stylus methods [3]. Full-field versions of this technique also exist, enabling two-dimensional data to be acquired from a single measurement. However, steep changes in surface gradient result in ‘shadowing’, because some areas of the surface are inaccessible to measurement. This also prevents triangulation systems from being able to look through holes to internal surfaces of the test piece.
Non-interferometric full-field methods include Moiré [4,5], Fourier transform [6,7] and fringe projection profilometry [8,9]. The resolution of Fourier transform methods is limited to around 1 mm. Moiré and fringe projection techniques, and the interferometric methods [10,11], are capable of higher resolution, but the diameter of the area under investigation is then often limited to a few centimetres. Discontinuities, or surface slope variations of more than an order of magnitude across the image region, compromise the performance of fringe methods, due to an inability to determine the fringe order at all positions [12].

[3] Author to whom correspondence should be addressed.

Interferometric techniques have the potential to provide absolute measurement of surface profile with micron scale resolution and centimetres of range. Both point and full-field implementations are possible. However, any techniques requiring an off-axis configuration, for which the illumination and observation axes do not coincide, suffer from shadowing problems.

Speckle interferometry is a generic term for a range of non-contact optical configurations that measure features of an object surface using the speckle effect, seen when an optically rough surface is illuminated by light coherent on the scale of the path differences corresponding to the surface roughness [13]. Although low-coherence interferometry has been in use for many years, its application in speckle interferometry techniques is much more recent [14,15]. The sources used can be relatively inexpensive, and good results can be obtained over a surface even if the slope varies widely in different regions of the image. Discontinuities in object height do not cause a problem. The use of optical fibres to replace bulk components in such systems typically increases portability and flexibility of deployment, and enables path-length matching to be achieved in compact arrangements, even for larger objects. Applications foreseen include quality control, solid modelling (the transfer of contour information to computer numerical control (CNC) machines) and measurement of surface wear due, for example, to erosion or corrosion.

In low-coherence speckle interferometry, light scattered from the object surface is mixed with a reference beam and imaged onto a CCD camera. If the optical paths for the object and reference beams match within the coherence length of the source, then interferometric speckles will be observed, the intensity of which are seen to modulate sinusoidally with changes in the reference path length [16]. The coherence length of an optical source correlates inversely with the spectral bandwidth [17]. A multimode diode laser with a bandwidth of a few nanometres has a coherence length of the order of 100 microns, while a true ‘white light’ source, such as a tungsten halogen bulb, has a coherence length of just a few microns. As the reference beam path is varied, interferometric speckles are seen along contour lines corresponding to the depth of the surface in the direction parallel to the optical axis [14]. The coherence length of the source determines the depth resolution, which is related to the width of the interferometric speckle contour lines.

Full-field low-coherence speckle interferometry has been demonstrated using a system called ‘light-in-flight’, which uses a pulsed source and time-gating [18]. Implementation was made difficult in this bulk-optic system because the long path lengths required to profile large objects necessitated construction of a very large instrument, not easily transported outside the laboratory environment. In this paper, we describe the development of optical fibre-based implementations of the low-coherence speckle technique, enabling compact, flexible systems to be constructed. A proposed configuration using a single axis for illumination and detection is discussed. This eliminates the shadowing problems encountered with techniques such as triangulation, and, provided that the axis of the hole is near-parallel with the optical axis, allows the system to see through a hole in the test surface.

2. Theory

The speckle effect is the granular appearance observed when a coherent source illuminates a surface rough on the scale of the illumination wavelength [19]. The speckle is caused by interference of light scattered from the object surface. The roughness results in path differences of the order of the wavelength. Over a localized region of space where the summed wave vectors remain approximately constant, the resultant intensity appears as a bright, a dark or a mid-tone speckle with a particular phase value.

The average dimension of a speckle is generally defined as the width of the autocorrelation function of the intensity distribution [20]. When a speckle image of the object is obtained using a lens, the resulting speckle pattern is termed ‘subjective speckle’ and the average speckle diameter S is given by

$$S = 1.22(1 + M)\lambda F \tag{1}$$

where M is the magnification of the imaging system, λ the source wavelength and F the f-number of the lens. This clearly gives the user some control over the speckle size by adjusting the size of the lens aperture; necessary to maximize the spatial resolution of measurements obtained from speckle images.

Low-coherence optical fibre speckle interferometry

The usual criterion for optimum resolution is to image one speckle onto one pixel of the CCD camera used for image capture [21].

Information about a surface is obtained by correlating fringes, usually obtained by subtracting one or more reference images from each of a set of phase-stepped interferometric speckle images and rectifying the resulting values before display [19]. This removes the random speckle phase information while retaining information about interferometer phase across the image. Correlation fringes can also be obtained by addition of the reference image to the phase-stepped images, but the correlation fringes are then superimposed on a dc term, which must be removed by filtering. The subtraction method is therefore considered preferable.

Parameters including shape [22], deformation [23], strain [24] or vibration [25,26,27] can be determined from the correlation fringe images. We consider first the situation of illumination by a high-coherence laser source. To extract the required information, two or more correlation fringe images obtained under different conditions must be combined, to yield information relating to the relative phases of corresponding speckles in each of the images. In profilometry, it is the shape of the object that is of interest. The usual technique is to acquire between three and five correlation images, for which the reference beam path length is altered by a known fraction of a wavelength between frames to introduce a known phase difference in the interferometer. This is known as 'phase stepping'. Simple algorithms exist [14,28,29], each suited to the number of phase steps employed, which enable the information from all acquired frames to be combined to extract either the amplitude or the phase of the correlation fringes. Usually, it is the phase that needs to be measured.

Given precise input data, those phase-stepping techniques that involve more steps lead to a more accurate phase measurement, since the sampling of the fringe pattern is better. Processing time increases with the number of steps, so a 3-step algorithm might be preferred where high speed processing is important. However, 4- and 5-step algorithms minimize sensitivity to any systematic error in the phase step. Following processing, a display of the image frame containing the calculated phase will show the phase modulo π, so a 'phase unwrapping' procedure is necessary to calculate the actual relative phase across the surface [30]. This often requires a degree of *a priori* knowledge about the form of the surface i.e. presence of discontinuities and sense of surface gradient.

The system described in this paper incorporates a broadband, low-coherence source rather than a single mode laser. This has implications for the appearance of the speckle patterns and the processing methods employed [14].

If we consider the basic speckle image acquired from a single frame of the camera, interferometric speckles occur only where the object and reference path lengths match to within the coherence length of the source. Thus, the correlation images appear dark except in these regions of interferometric speckle. Here, the speckles will modulate with varying amplitude as the reference path length is scanned, the visibility reaching a maximum for zero path-length imbalance. Thus if the bandwidth of the source is chosen to ensure a very small coherence length, for example a few tens of microns, the depth co-ordinate of any point on the measured surface is determined, with high resolution, from the position of maximum fringe amplitude. In low-coherence speckle interferometry (LCSI), the amplitude, rather than the phase, is therefore the parameter of interest. For this reason, LCSI is an absolute measurement method, since amplitude, unlike phase, is determined uniquely and absolutely from the phase-stepping algorithm. The depth resolution obtained from the system depends on the source coherence length and the ability of the detection system to identify correctly the central fringe within the coherence envelope as the reference path is scanned.

3. System components

3.1. Source considerations

Since the depth resolution of a LCSI system is dependent primarily upon source spectral profile, the choice of broadband source is of critical importance in obtaining the best performance from the instrument. Sources that have been employed for low-coherence interferometry include thermal types, e.g. tungsten halogen lamp [31], discharge lamps such as mercury or xenon lamps [32], light-emitting and superluminescent diodes (LEDs and SLDs) [33] and multimode laser diodes (MMLDs) [34]. The first two of these are true 'white light' sources with bandwidths in excess of 1000 nm, from the ultra-violet through to the infra-red (IR). The others have bandwidths typically of several tens of nanometres and operate in the visible and IR. LEDs generate photons through spontaneous emission and typically have a low power output. SLDs are similar but use a higher current density so that the power available is much higher. MMLDs generate stimulated emission and have cleaved facets to the chip, which form an optical resonator cavity. This feature also accounts for the typical structure of the MMLD spectrum, which comprises a series of narrow peaks within an envelope profile. Recently, super-continuum sources have been developed, based on photonic crystal fibres, with bandwidths of over 100 nm. These have been demonstrated in optical coherence tomography [35]. However, they are generally expensive and rather bulky, as they require a pump laser.

Of the source types described here, all could potentially be employed in a LCSI system, although the low power output of LEDs is likely to limit their usefulness. Additional criteria apply, however, in a fibre-based system. True white light sources seem initially very attractive as they have a coherence length of no more than a few microns, but the coupling efficiency from this type of source into single-mode optical fibre is extremely low, rendering them unsuitable for consideration.

The experimental work for this project was carried out shortly before high-power, broadband superluminescent sources became widely available. Although coupling efficiency into fibre is much higher for LEDs and SLDs due to the spatial coherence of the beam, the limited power obtained until recently from devices of this type meant that they could be used in fibre-based systems only for examination of very small objects. The maximum power available from an SLD was then about 1 mW, whereas it has recently become possible to obtain SLDs with powers in excess of 30 mW and bandwidths of about 50 nm, making them more attractive for use in low-coherence systems.

In this work, the use of Sony 201V-3 (40 mW) and 202V-3 (20 mW) MMLDs was investigated, with wavelengths close to 800 nm. The coherence length was measured as the FWHM of the interferogram obtained by inserting the source into a scanned Michelson interferometer with one reflector mounted on a moving translation stage, and was found to be 40μm for the 201V-3 source run below threshold, and 150μm above threshold. Although the spectral widths of multimode laser diodes are thus less appropriate for high-resolution LCSI than those of SLDs, MMLDs were selected for the systems detailed in this paper because they offered the best combination of relatively high power, up to hundreds of milliwatts for the most powerful devices, and spectral bandwidth. Additionally, the coupling efficiency into singlemode optical fibre is good. Measures were introduced in this project to reduce the undesirably high degree of coherence and to exploit the comb-like spectral structure to improve resolution. These are discussed below in more detail.

3.1 Source selection for fibre-based low-coherence speckle systems

The combination of two monochromatic sources of different wavelengths λ_1 and λ_2 results in a beat wavelength [36]

$$\lambda_{synth} = \frac{\lambda_1 \lambda_2}{|\lambda_1 - \lambda_2|} \tag{2}$$

known as the 'synthetic wavelength'. For broadband MMLD sources, the spectral distribution of the synthetic wavelength is also broadened, leading to a decrease in the coherence length, but the mean value

can be obtained as before by substituting the mean values for the individual sources into the above equation.
Maximising the intensity difference between the central fringe and the two adjacent fringes eases correct identification of the central fringe in an interferogram formed from combined sources. This requires the central fringe packet in the envelope of the synthetic distribution to be very narrow. Ideally, only 3-5 fringes should fall within the central packet. Calculation of the synthetic distribution satisfying this requirement leads to an optimum separation between the mean wavelengths for the two sources, which are assumed to be of equal, known coherence length [37]. For the optimum wavelength combination, the intensity of the central fringe must also be equal in each of the two combining spectral distributions to obtain the best possible signal-to-noise ratio.
Combined MMLDs were investigated experimentally, and proved very effective in bulk-optic LCSI, in improving the depth resolution of the system. However, in the subsequent fibre-optic based systems it was found that no wavelength beating occurred between the two sources and, instead of the expected periodic beat pattern, a single pair of broad, bright fringes was seen in the images. This can be explained as a consequence of the material dispersion of the glass fibres, in which the refractive index, and therefore the optical path difference, is dependent upon the transmitted wavelength. It can be inferred that spatial resolution problems will also be experienced with very broadband single sources. Although the reduction in coherence length with increasing source bandwidth reduces the SNR required to identify the central fringe, the correlation fringes will appear broadened in the images because of the dispersion, reducing spatial resolution in the plane perpendicular to the optical axis.
The dispersion could, in principle, be compensated, at the expense of increased complexity of the system, but it was considered preferable in this project to employ a single MMLD source for fibre-optic systems.

The possibility of using pulsed MMLDs was also investigated. Pulsing broadens the spectrum while retaining a high optical power output. This has previously been used in absolute distance measurement applications [38]. The pulse broadening occurs because of refractive index changes in the laser cavity, due to a combination of carrier density fluctuations and thermal effects. For small signal modulation frequencies the thermal effect is dominant, whereas at frequencies in the GHz range the carrier density is more important. Pulsing was achieved using a function generator to modulate the diode. A sinusoidal pulsing signal of amplitude 50mA was imposed in addition to a DC bias current of 100mA. The diode spectrum was observed by coupling the beam into an optical spectrum analyser via a length of single mode fibre.
Pulsing was investigated using a 20 mW Sony SLD202V-3 multimode laser diode at 812 nm. Laser spectra are shown in figure 1(a) and (b) for both cw operation and for pulsing at 100 Hz. The ratio of power obtained under pulsed operation to that measured under cw operation is 0.32, and the FWHM spectral width, derived from a Gaussian fit to the spectrum, increases from 3.2 ± 0.5 nm to 4.0 ± 0.5 nm. The lasing mode width also increases considerably due to the pulsing, smoothing the overall spectrum.
The calculated coherence length for the laser in pulsed mode is reduced by a factor of 1.2 compared with the cw coherence length, from 206μm to 165μm. Figure 1(c) and (d) show the effect of pulsing on the visibility of correlation fringes generated from a tilted circular plate. The multiple bright lines represent peaks in the correlation envelope. The intensity of the central fringe packet relative to its immediate neighbours is enhanced by pulsing, and the intensity of the peripheral fringes drops off more rapidly, reducing the total number of visible fringes across the image. Note that the fringe packet *spacing* is unchanged, in accordance with theory.
A form of source noise, known as “laser partition noise”, results from variations in the relative intensity of modes of the lasing spectrum with time [39]. It was found to be beneficial to average the interferogram over a number of images. The effect is to cancel any noise caused by random variations in spectral shape from pulse to pulse. The optical power output from a pulsed MMLD is of the same order of magnitude as that from the laser run under cw operation. Thus the pulsed MMLD provided the best overall performance as a source for fibre-based LCSI, and was the source used in all subsequent experimental designs.

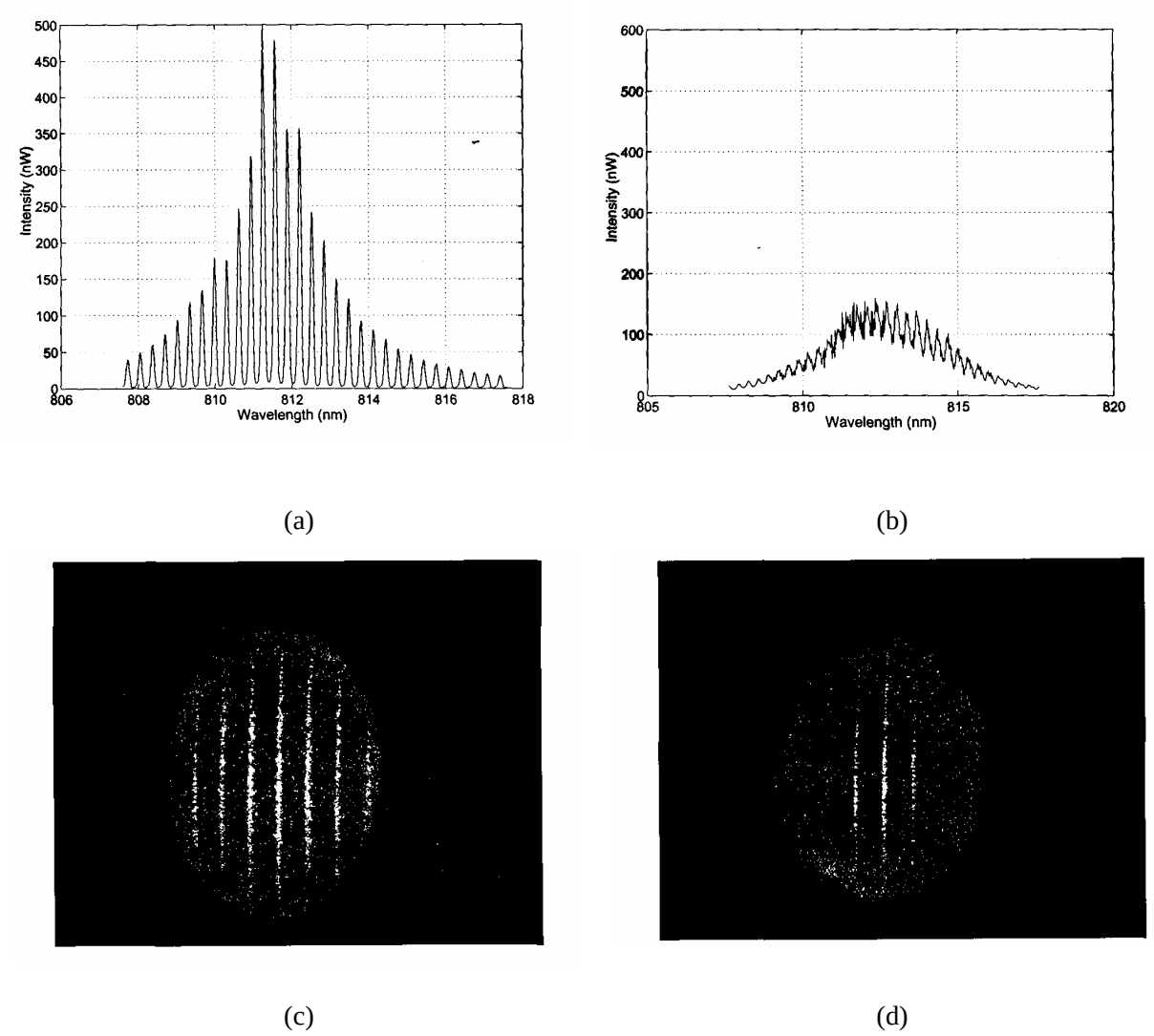

Figure 1. Intensity spectra of Sony SLD202V-3 multimode laser diode operating in (a) cw mode and (b) pulsed mode at 100 Hz. The lower images show correlation images obtained from a metal plate, tilted about a vertical axis, under (c) cw and (d) pulsed illumination.

3.2 Detector

The detector for the results displayed in this paper was an 8-bit analogue CCD camera. A 12-bit digital camera was investigated for comparison to assess the significance of pixel noise and digitization noise on the overall measurement precision. However, no discernible improvement in performance was obtained by using the higher specification camera, implying that, for these measurements, thermally-induced changes in speckle intensity between frames are more significant in the overall measurement uncertainty than any noise introduced by the detector. The digital camera did offer the advantage of longer image integration times, improving signal intensity towards the edges of the images.

4. A low-coherence fibre speckle interferometer (LCFSI) for 3D shape measurement

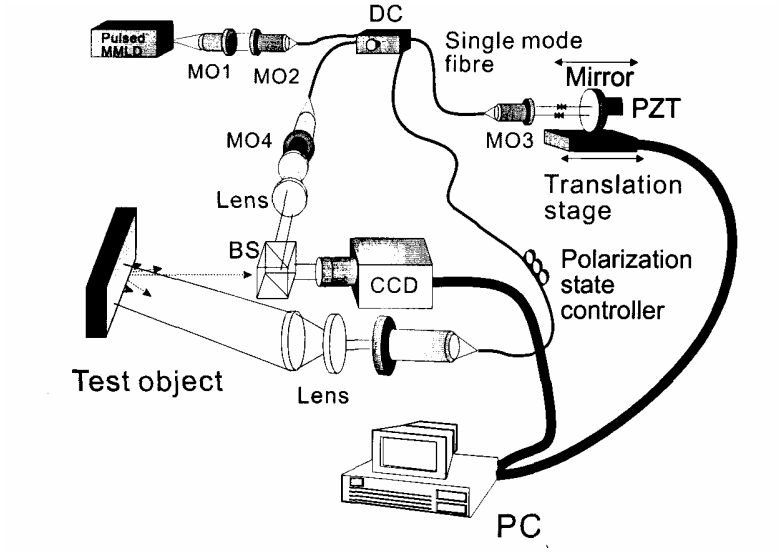

Figure 2. Design for optical fibre-based LCFSI system, using collimated illumination and reference beams. MMLD: multimode laser diode, MO1,2: microscope objectives to couple light from the source into fibre, MO3,4: microscope objectives for beam collimation, DC: directional coupler, BS: beam splitter, PZT: piezoelectric mirror mount.

During the development of a LCFSI for 3D shape measurement, several experimental configurations were investigated. The basic design is shown in figure 2. Light from a MMLD was coupled into a fibre directional coupler (DC) with an 80/20 split ratio. One output of the coupler was used to illuminate the test object. About 3-5 mW of optical power illuminated the object surface. The output from the other arm of the coupler was collimated and retro-reflected by a plane mirror mounted on a computer-driven translation stage. The hysteresis of the translation stage was assessed by repeating a profile measurement twice while scanning the translation stage in opposite directions for the two scans. No detectable hysteresis was discovered.

The reflected light was re-coupled into the system and transmitted through to the fourth port of the coupler, where a beam splitter was used to direct the ouput beam into the CCD camera. This constituted the reference beam. The reference and signal beams combined in the camera plane to create the interferogram, which was acquired and displayed by the PC. However, induced birefringence arising from fibre deployment leads to differing states of polarization in the signal and reference arms of the system. A coiled-fibre polarization state controller, positioned in the illumination fibre, was therefore used to adjust the state of polarization and prevent signal fading. Depolarisation of light can occur on scattering from an optically-rough test object, but this is not generally a major problem for singly scattering surfaces, such as the lightly abraded metal surfaces investigated here, at near-normal incident angles [40]. Employing fibre increases the flexibility of the system as a whole since it is no longer necessary to ensure precise matching of “air paths” in the interferometer. Approximate matching of the lengths of optical fibre is more straightforward, and the final correction required can be achieved using a short, adjustable air path.

Initially, the collimating lenses were omitted from both illumination outputs of the coupler. Given sufficient source power, it is possible to investigate large objects using this system, because the beams from the fibres are divergent. However, the spatially-dependent path length differences between the signal and reference beams produce concentric circular fringes for a flat plate object at typical working distances. This does not prevent use of the system, but interpretation of the correlation fringes requires additional computation, and requires accurate measurement of several parameters related to the

experimental geometry. The original design was therefore modified to include the additional lenses, as shown in figure 2. Both object and reference beams were now collimated as they left the delivery fibres. Although illumination of large object areas using this modified system requires similarly large, and costly, collimation optics, there is an advantage in the removal of spurious circular fringes from the interferogram. It should be noted that the illumination for these systems is slightly off-axis, which must be accounted for in calculating the surface profile.

An on-axis implementation of the system could be realized, by using a polarizing beamsplitter (PBS), and arranging for signal and reference beams with a common polarisation to enter opposing faces of the PBS. The counter-propagating signal and reference beams are both reflected, and therefore separated by the PBS, with an appropriately oriented quarter wave plate positioned in the path of the signal beam to rotate the polarization state through 90^o following a double pass through the component. The returning signal beam is now transmitted by the PBS, and a polariser is positioned in front of the detector at 45^o to both beams to enable interferometric mixing on beam recombination at this position. The on-axis version of the system would avoid any shadowing problems that could be encountered with sharp changes of gradient of the object surface, and would allow the system to look through holes in a test piece to internal surfaces below.

Equalization of the optical path lengths in the interferometer arms was realized by inserting a single-mode laser diode as the source. Modulating the optical frequency of the laser diode produces a phase change in the interferometer when a path length imbalance exists. This method has been used to measure path-length imbalance in fibre ESPI systems [41]. The interferometer can be balanced to within a centimetre or so by minimising the phase change, and final searching for the coherent interferogram can be performed by translating the stage-mounted mirror under computer control.

4.1 Image processing

Many computational techniques exist for extraction of the fringe amplitude from speckle interferograms. However, the Hariharan [42] or five-step technique has the advantage that errors due to miscalibration of the selected phase step can be minimized, if a step value of $\pi/2$ is chosen. The expression for the fringe amplitude then becomes

$$A(x,y) = \frac{1}{4}\sqrt{4(I_4 - I_2)^2 + (I_1 + I_5 - 2I_3)^2} \tag{3}$$

A PC running LabView™ was used to control acquisition, since the program enabled synchronization of the translation stage, camera and PZT to allow automated data processing. Five images were acquired and smoothed using a median filter. For each pixel, the amplitude *A(x,y)* was determined. Acquisition and smoothing was repeated 10 times and the results averaged, to remove the effects of random fluctuations in the pulsed laser spectrum. After averaging, the contour depth was calculated. Consecutive frames containing values of the averaged fringe amplitude were compared to find the maximum within the mirror scan range for each pixel. A depth value was then assigned to the pixel from the mirror position associated with this frame.

4.2 Temperature sensitivity

The thermal expansion of silica and its refractive index sensitivity can lead to phase variations of the guided beam with temperature. At a wavelength of 800 nm, the thermal phase change for this type of fibre is about 190 rad $^oC^{-1}m^{-1}$, with the major effect being refractive index variation rather than thermal expansion. Although the phase is not measured using LCFSI, any phase variations can affect accuracy since the fringe amplitude measurement relies on a phase-shifting method. Both fibre arms of the interferometer are constructed of the same type of fibre. Therefore, if the same temperature change affects both arms, the important parameter is the *difference* in length between the two fibres, which for our system was 0.28 m. Thus the phase variation due to temperature can be calculated as 53 rad $^oC^{-1}$. This

represents a movement of about 9 fringes for a 1°C rise in temperature, and implies that the system should be packaged in an insulating enclosure to avoid problems of fringe drift.

4.3 Depth of field

Since three-dimensional objects are imaged using the LCFSI technique, the depth of field of the imaging system is an important consideration. Poor depth of field can lead to reduction in fringe visibility and hence to a reduced SNR. Depth of field is inversely related to the light-gathering power or F-number of the lens, and a compromise will generally be necessary between the two. In our system, a zoom lens with the focal length *f* variable between 28 and 70mm was used as the imaging optic. The depth of field was calculated from the lens parameters, using an assumed object distance of 400mm, to be 44mm for *f*=28mm, and 8mm for *f*=70mm.

Assuming the worst-case depth of field for the system, defocus will occur for an object where the variation in surface contour is more than 8mm. This was not a problem for the objects examined in the present study. However, for large object tilts or surface curvature, defocus could become important. There are two ways of overcoming the problem; one is to divide the surface into smaller regions, each of which can be imaged without excessive defocus by adjusting the focusing condition of the lens. The other solution is to employ telecentric lenses, which provide a constant magnification over the entire field of view, and have a typical depth of field up to about 50mm. The disadvantage of telecentric systems is that the maximum object size is fixed and is typically rather small at less than about 100mm [43].

4.4 Measurements on a circular plate made using the LCFSI

The test object used was a circular plate, 20 mm in diameter, made from stainless steel polished to a surface roughness of about 2μm. No additional surface finish was applied during measurements on this object. Figure 3 shows a typical set of correlation fringes obtained for a tilt applied in the horizontal direction, and figures 4(a) and (b) depict 3D mesh graphs before and after application of a filter to remove spurious peaks caused by incorrect identification of the central fringe. Selection of an appropriate filter here is of great importance, in order to remove spurious peaks without also removing true features of the object. For example, a discontinuous step may exist on the object surface. To distinguish this from a spike on a single pixel, a neighbour comparison can be applied over a small region of pixels. A pixel within the region, which differs in depth from a certain number of its neighbours by more than a pre-selected value, is discarded. If the threshold number of required neighbours is taken to be at least half of those in the region, erosion of the image edges will be avoided. The maximum desirable gradient of the measured surface (disregarding step changes) is one mirror step per pixel. Therefore, if a neighbourhood comprises a region of 5x5 pixels, a maximum allowed pixel-to-pixel depth variation can be defined at slightly more than four times the mirror step. This is the process that has been applied to figure 4(a), resulting in 4(b). The removal of the peaks produces “gaps” in the data corresponding to the unusable pixels. These can be filled by interpolation to improve the appearance of the final profile image.

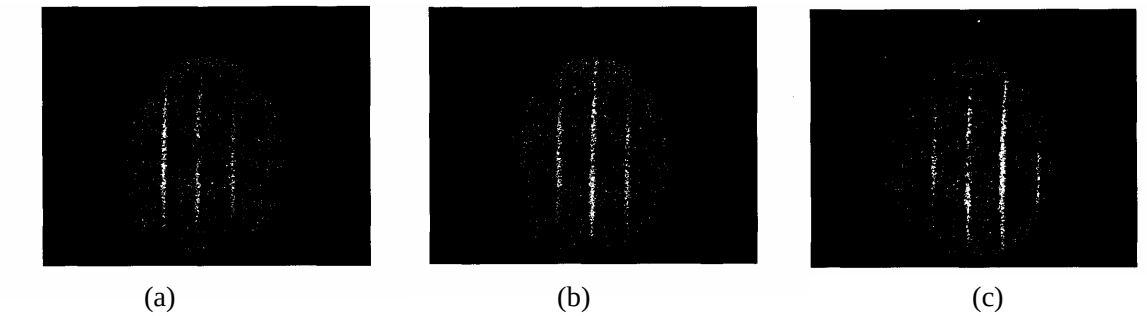

(a) (b) (c)

Figure 3. Correlation fringes obtained from a stainless steel plate, tilted slightly in the horizontal direction, under pulsed illumination from a MMLD. The images illustrate the movement of the brightest fringe from (a) left to (b) centre and finally (c) right of the image as the reference mirror is scanned.

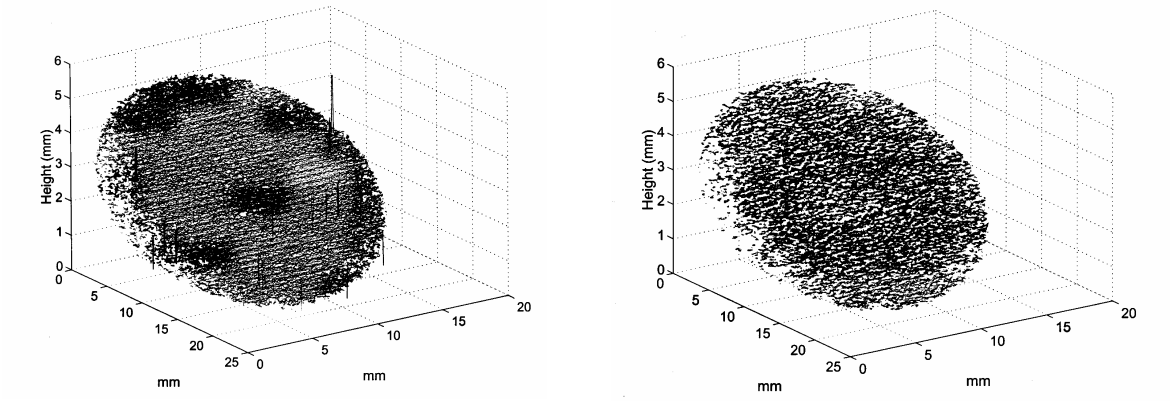

(a) (b)

Figure 4. Mesh plots of a tilted plate under pulsed illumination, calculated using the Hariharan 5-step algorithm, showing (a) unfiltered data and (b) data after appropriate filtering to remove spikes.

Profiles, shown in figure 5, were acquired for tilt angles of $10^o \pm 0.5^o$, $20^o \pm 0.5^o$ and $30^o \pm 0.5^o$ relative to the camera plane, determined by applying trigonometry to distances measured on the optical table.

The interferometrically measured tilt was obtained in each case by fitting a plane to the acquired profile, using a least-squares method, and the resulting values were $5.62^o \pm 0.04^o$, $16.19^o \pm 0.04^o$ and $26.46^o \pm 0.04^o$. There is an average systematic error angle of 4.0^o, which corresponds to half the illumination offset angle of 8^o. When a correction is applied for this, interferometrically measured tilt values are in good agreement with the independent measurements.

From figure 5, it can be seen that the number of unusable data points increases with tilt angle, because the scattered optical power collected by the camera is reduced. However, the data acquired are sufficient to define the surface even at the highest tilt angle of 30^o. A second set of measurements was made for an illumination angle of 11^o, and the systematic error angle was now found to be 5.5^o, confirming the geometrical interpretation of this offset.

The uncertainty in the measurement of surface depth, calculated as the standard deviation of the sample data from the fitted plane, is about ±20μm.

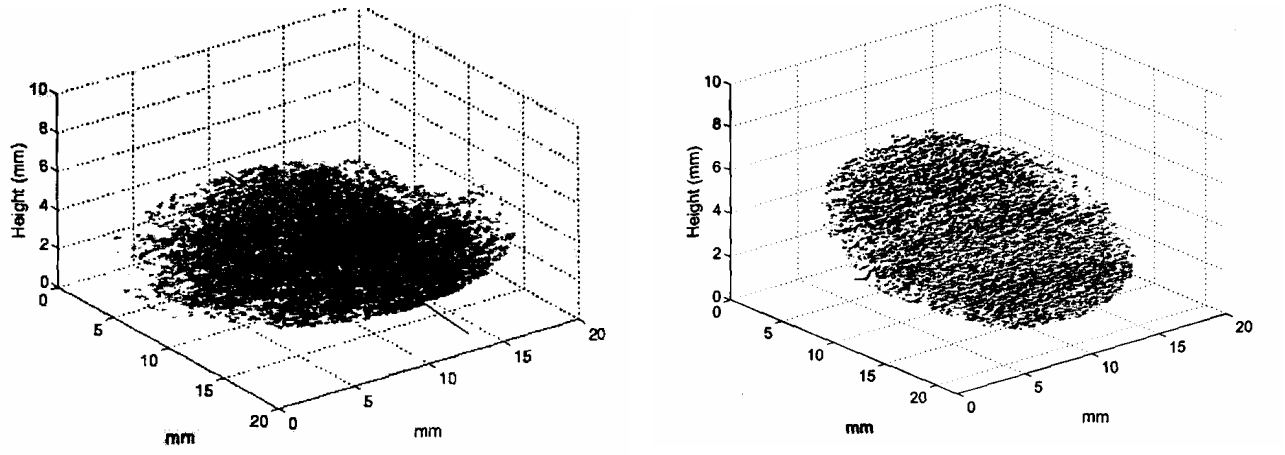

(a) (b)

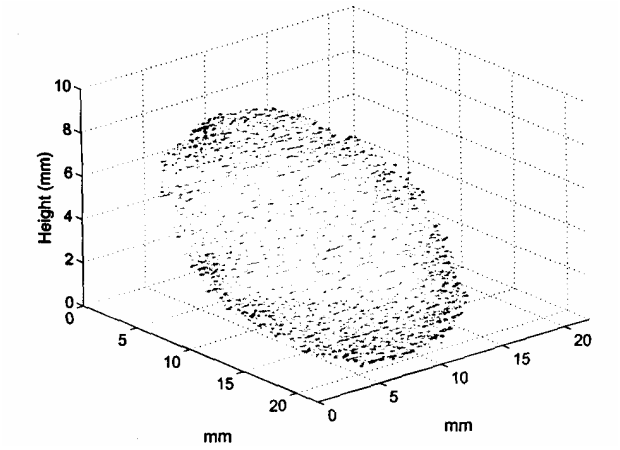

(c)

Figure 5. Filtered mesh plots of a tilted plate under pulsed illumination, calculated using the Hariharan 5-step algorithm, for tilt angles of (a) 10^o (b) 20^o and (c) 30^o.

5. Polarization-maintaining low-coherence fibre speckle interferometry (PM-LCFSI)

The fibre systems described above are constructed from standard single-mode optical fibre. A common problem encountered with optical-fibre interferometric systems is drifting of the polarization state, resulting from birefringence induced in the fibres by bending or pressure stresses due to the deployment of the fibre. The induced birefringence causes a random variation of the preferred polarization axes which, when the reference and signal beams propagate in different fibres, can result in the polarization states of the two interfering beams becoming mismatched or even orthogonal, with a consequent reduction or loss of the interference signal. The signal intensity is also time-varying because of changes in fibre deployment conditions and ambient temperature.

Mounting sections of the fibre interferometer arms on polarization state controllers and adjusting these to correct for changes in polarization can reduce signal fading. This solution, however, requires a monitoring and feedback control circuit for correction of the polarization state, which considerably increases the complexity of the optical system.

An alternative solution is to construct the optical system using polarization-maintaining fibre. The polarization state of light propagating in a linear polarization mode of the fibre will then be unaffected by environmentally-induced changes. All fibre components, such as couplers, must also be polarization maintaining, which increases the cost of the system. However, such components are not unduly expensive.

A modified version of our LCFSI system was constructed using Fujikura PANDA-type polarization-maintaining fibre with a beat length of 3 mm. It was also considered that mounting a reference mirror on the object would offer advantages. It eases the setting up process required to ensure path-length matching in the interferometer, and relaxes the stability requirements between the interferometer and the test object, due to the high degree of common-mode rejection obtained using this configuration. It also reduces considerably the lengths of fibre required in the reference arm to match the object arm path length. As the object-to-instrument distance is changed, the local reference beam compensates for this and no additional fibre is required in the reference path to reach approximate path length balance. Figure 6 shows the experimental arrangement of the system, with a small reference mirror mounted on the test object. Ideally, the reference beam would be generated from scattered light gathered directly from a point on the object surface in a similar way to that used in a fibre optic ESPI vibration sensor [44]. For some surface finishes this might be possible, but in our case it was found to produce insufficient power in the reference beam.

Light propagating via DC1 and DC2 is focused onto the object-mounted mirror. Reflected light, coupled back into the same fibre, propagates via DC2 and DC3 to a second, stage-mounted reference reflector, to allow scanning of the reference path length. Reference and signal light then recombine at the beamsplitter, forming an image on the CCD camera.
The fibre arms of the polarization-maintaining couplers, which were fabricated in our laboratories using the polished half-block technique [45], were fusion-spliced to construct this system, using an arrangement incorporating a rotating chuck to match the polarization axes of the spliced fibres.

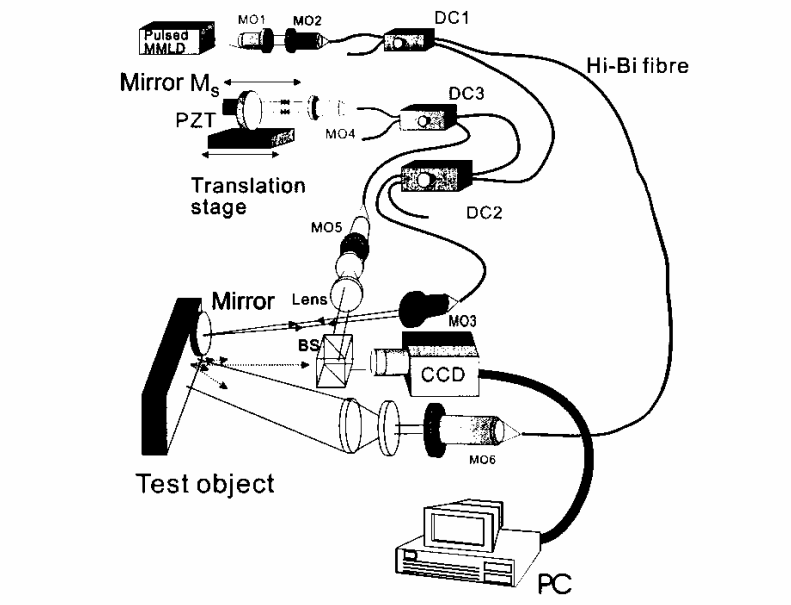

Figure 6. Configuration for optical fibre-based PM-LCFSI system, with object-mounted reference mirror. MMLD: multimode laser diode, MO1,2: microscope objectives to couple light from the source into fibre, MO3: objective for focusing reference beam onto object, MO4,5,6: objectives for beam collimation, DC1,2,3: polarization-maintaining directional couplers, PZT: piezoelectric mirror mount.

5.1 Measurements on test objects using the PM-LCFSI
Test objects were investigated with the polarization-maintaining system, including a tilted metal plate as before, a coin and a stepped test piece. The aim of these measurements was to compare the resolution of the polarization-maintaining system with that of the system constructed from standard fibre. All procedures used to compare experimental and theoretical data were as for the previous measurements in section 4 above.

5.1.1. Tilted plate. Measurements on the tilted plate were repeated at mirror-step intervals of 10, 5 and 2μm, to investigate the effect of the different sampling intervals on the results obtained. The object-mounted mirror places an additional constraint on the measurements, since a sufficient fraction of the optical power reflected by the reference mirror must be collected to constitute a useful reference beam. This limits the angle of tilt that can be tolerated in the region where the reference mirror is mounted. A miniature corner cube could be used instead of the mirror to remove this limitation. The object tilt as measured from the system geometry was $-1^{o} \pm 0.5^{o}$.
The test object was tilted slightly during measurement to avoid specular reflections into the camera. Profiles were acquired for the three different step intervals, and the corresponding values for the interferometrically measured tilt and the uncertainty in depth measurement are given in table 1.

Agreement with the independent measurement of angle is good in all cases, but the measurement accuracy appears to be independent of the step interval chosen. This implies that other sources of error, such as speckle noise and laser noise, cause uncertainties in measured depth that are greater than the largest step interval investigated. The uncertainty in the depth measurement for the PM-LCFSI system is about 14μm, compared with the best value measured for the standard fibre system of about 20μm. This improvement is commensurate with a reduction in intensity variations resulting from the elimination of polarization-based signal fading.

Table 1. Object tilt and depth error for a tilted plate, measured from profiles acquired using the PM-LCFSI system.

Mirror step	Total tilt (degrees)	Depth error (μm)
10	-0.68 ±0.50	13.4
5	-0.69 ±0.50	13.6
2	-0.71 ±0.50	13.9

There is a difference in the appearance of profiles obtained using the three different step intervals. More 'gaps' in the data are seen when the step size is larger. These represent areas where no valid data was collected. With a smaller step interval, the density of data collected is greater, and therefore the total number of 'valid points' is higher. This must be borne in mind when profiling objects with a highly detailed surface structure.

Alignment of this interferometer system was expected to be much easier than for the earlier version. To demonstrate this feature, the distance between the camera and the test object was changed, causing a loss of path balance and therefore of interference fringes. Adjustment was then carried out until interference fringes could once again be seen in the images. Even following a relatively large movement of the object (about 40mm), minimal adjustment was required to retrieve the fringes, consisting primarily of re-focusing the reference beam onto the miniature mirror at its new location. It is advantageous that the stage-mounted mirror no longer has to be translated many millimetres to a new position, which can necessitate troublesome re-alignment to re-optimize the fibre coupling in this section. It also allows a stage with much shorter travel range to be used, encompassing simply the maximum object depth expected.

5.1.2. Five pence coin. A CCD image of a UK five pence coin under white-light illumination is shown in figure 7(a). The diameter of the coin is 18mm. Initially, problems were encountered in obtaining a profile, due to specular reflections from some regions of the coin saturating areas of the camera image. Tilting the coin helped, but did not completely eliminate the specular reflections. Immersing the coin in a weak acid solution for an hour to etch the surface was found to alleviate the problem. Surface characteristics are always a consideration in speckle-based profiling systems, since roughness at or greater than the scale of the illumination wavelength is required for speckle formation.
A profile was measured with a mirror step of 5μm. Figure 7(b) shows a three-dimensional mesh plot. The black regions towards the base of the coin, around the neck of the Queen's head and between the letters

correspond to patches of data that are missing after application of the noise filter algorithm. However, data density was generally good, and a profile was obtained with a precision of about ±16μm.

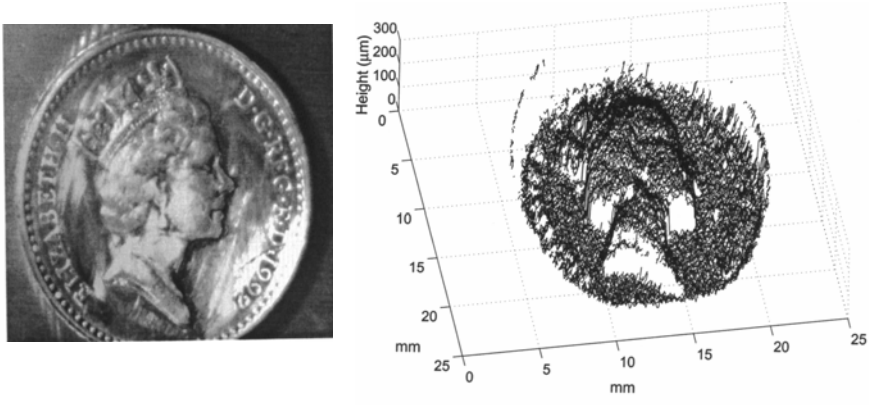

(a) (b)

Figure 7. (a) Photographic image taken in white light and (b) 3D mesh plot acquired using PM-LCFSI of a UK 5 pence coin, 18 mm in diameter. The surface of the coin has been etched in a weak acid solution.

5.1.3. Stepped test piece. The test object, shown in figure 8, consisted of a cylindrical aluminium bar, 1 cm in diameter, the end of which was machined to produce a series of four concentric circular steps. As shown in the figure, the reduction in diameter between levels was 2 mm, and the step positions relative to the top surface were, respectively, –40 ± 2μm, -70 ± 2μm and –90 ± 2μm, obtained from machining tolerances.

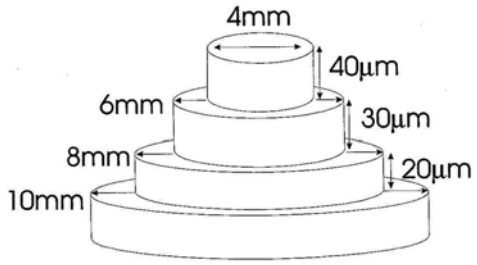

Figure 8. Schematic of stepped test object, made from a machined aluminium bar.

The object was profiled using the PM-LCFSI system with a sample interval of 10μm, so that the results could be compared with those from the standard fibre LCFSI system using the same step interval. Once again, there were some problems with specular reflections saturating regions of the camera, and this is characterized by rather sparse data density within a narrow 'bow-tie' shaped region across a diameter of the mesh profile shown in figure 9. Planar equations were fitted to the data from each level, and the standard deviation in the depth of the fitted plane was found to be about 11μm. Measured step heights agreed with independent measurements, taking into account this uncertainty, which is comparable with the step interval of 10μm.

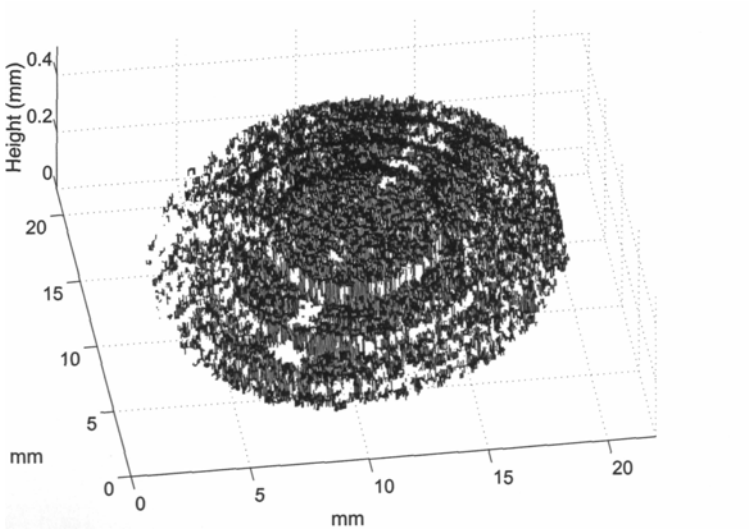

Figure 9. 3D mesh plot acquired using PM-LCFSI of the stepped test piece, with a step interval of 10μm.

5.2 Temperature sensitivity

Temperature sensitivity was once again a concern in this system. Since light propagates in only one linear polarization mode of the polarization-maintaining fibre, the temperature stability calculation is essentially identical to that used in assessing the standard fibre system, and the normalized sensitivity has the same value of 190 $rad^{o}C^{-1}m^{-1}$. Coincidentally, the mismatch in fibre lengths is also very close to that for the standard fibre system, and so the temperature sensitivity turns out to be about the same, at 57 $rad^{o}C^{-1}$. We therefore conclude once again that, for optimum stability, the polarization-maintaining fibre system should be enclosed in a temperature-stable environment provided by hermetically-sealed packaging.

As discussed in section 3.1 above, alternative optical sources have become available over the last few years, with excellent characteristics for use in low-coherence systems. These include both the new generation of superluminescent diodes, available with bandwidths up to tens of nanometres for powers up to about 50 mW, and supercontinuum sources with bandwidths in excess of 100 nm. Such sources could replace the pulsed MMLD in the profiling systems described in this paper, and would be likely to lead to an increase in depth resolution and improved signal-to-noise performance.

6. Conclusions

The use of optical fibre components in low-coherence speckle interferometry has been shown to alleviate many of the experimental difficulties encountered in constructing bulk-optic systems. Optical path lengths much greater than the actual physical path lengths within the system can be achieved without difficulty, allowing larger objects to be illuminated with fibre-based systems. Long path-length interferometers constructed using fibre are also less susceptible to disturbances caused by vibration or mechanical instabilities of the optical mounts. Path-length matching between the signal and reference arms is achieved more readily, and portable, flexible, small ‘footprint’ instruments can be constructed. On-axis implementations of fibre systems are possible, which will allow these systems to see through holes in the test surface, to any additional surface below.

The main disadvantage of fibre implementations is their greater sensitivity to ambient temperature fluctuations than the bulk-optic systems. However, this can be minimized by enclosing instruments in thermally insulated enclosures, or by employing a phase-control feedback system [46]. The optical

dispersion of the fibres will limit resolution for very broadband sources. However, for the source bandwidths used in this study, laser noise and not dispersion was the limiting factor on resolution.
The system constructed from polarization-maintaining fibre offers the additional advantage of eliminating signal fading, caused by a relative drift between the polarization states of signal and reference beams. If the reference mirror is mounted on the test object, problems caused by bulk motions of the test piece relative to the interferometer are also eliminated, resulting in a more rugged system, and the path-length matching condition can be recovered with only slight readjustment when the test object is changed or moved.
The experimental measurements presented in this paper, using a pulsed MMLD source with a coherence length of about 165 μm, have demonstrated a depth resolution of ±20 μm for the standard fibre system described, and a resolution of ±14 μm for the system based on polarization-maintaining fibre. The improvement seen for the polarization-maintaining system is attributed largely to the elimination of noise in the images due to polarization variations. The depth ranges of our systems were limited by depth of focus of the imaging system or by the scanning range of the translation stage used for path matching.

Acknowledgments
This work was supported by a grant from the Royal Society UK.

7. References
[1] Chen F, Brown G M and Song M 2000 Overview of three-dimensional shape measurement using optical methods *Opt. Eng.* **39** (1) 10-22.
[2] Malacara D 1992 Contact and non-contact profilers *Optical Shop Testing* (New York: Wiley) 687-714
[3] Hasman E, Keren S, Davidson N and Friesem A A 1999 Three-dimensional optical metrology with color-coded extended depth of focus *Opt. Lett.* **24** (7) 439-41
[4] Trolinger J D 1996 Fundamentals of interferometry and holography for civil and structural engineering measurements *Opt. Laser. Eng.* **24** (2-3) 89-109
[5] Moore D T and Truax B E 1979 Phase-locked Moiré fringe analysis for automated contouring of diffuse surfaces *Appl. Opt.* **18** (1) 91-6
[6] Takeda M and Mutoh K1983 Fourier transform profilometry for the automatic measurement of 3d object shapes *Appl. Opt.* **22** (24) 3977-82
[7] Takeda M, Gu Q, Kinoshita M, Takai H and Takahashi Y 1997 Frequency multiplex Fourier transform profilometry: a single-shot three-dimensional shape measurement of objects with large height discontinuities and/or surface isolations *Appl. Opt.* **36** (2) 5347-54
[8] Srinivasan V, Liu H C and Halioua M 1984 Automated phase-measuring profilometry of 3D diffuse objects *Appl. Opt.* **23** (18) 3105-8
[9] Su X Y, von Bally G and Vukicevic D 1993 Phase-stepping grating profilometry: utilization of intensity modulation analysis in complex objects evaluation *Opt. Comm.* **98** 141-50
[10] Groves R M, James S W and Tatam R P 2004 Shape and Slope measurement by source displacement in shearography *Opt. Laser. Eng.* **41** 621-34
[11] Tatam R P 1999 Optoelectronic Speckle Interferometry: Recent developments and applications *Proc. Interferometry '99 (Warsaw,Poland)* SPIE 3745 114-33
[12] Takeda M and Yamamoto H 1994 Fourier-transform speckle profilometry: three-dimensional shape measurements of diffuse objects with large height steps and/or spatially isolated surfaces *Appl. Opt.* **33** (34) 7829-37
[13] Ennos A E 1997 A look back at the early development of speckle metrology *Opt. Laser. Eng.* **26** 87-92.
[14] Dresel T, Häusler G and Venzke H 1992 Three-dimensional sensing of rough surfaces by coherence radar *Appl. Opt.* **31** (7) 919-25
[15] Lee B S and Strand T C 1990 Profilometry with a coherence scanning microscope *Appl. Opt.* **29** 3784-8

[16] Butters J N and Leendertz J A 1971 Speckle pattern and holographic techniques in engineering metrology *Opt. Laser. Technol.* **3** (1) 26-30
[17] Born M and Wolf E 1993 Interference and diffraction with partially coherent light *Principles of Optics* sixth (corrected) edn (Oxford: Pergamon Press) 491-554
[18] Carlsson T E and Nilsson B 1998 Measurement of distance to diffuse surfaces using non-scanning coherence radar *J. Opt.* **29** (3) 146-51
[19] Jones R and Wykes C 1986 Speckle pattern interferometry *Holographic and Speckle Interferometry* second edn (Cambridge: Cambridge University Press) 165-96
[20] Ennos A E 1984 Speckle Interferometry *Laser Speckle and Related Phenomena* (Berlin: Springer-Verlag) 207-8
[21] Løkberg O J, Seeberg B E and Vestli K 1997 Microscopic video speckle interferometry *Opt. Laser. Eng.* **26** 313-30
[22] Tatam R P, Davies J C, Buckberry C H and Jones J D C 1990 Holographic surface contouring using wavelength modulation of laser diodes *Opt. Laser. Technol.* **22** 317-21
[23] Leendertz J 1970 Interferometric displacement measurement on scattering surfaces utilizing speckle effect *J. Phys. E.: Sci. Instrum.* **3** 214-8
[24] Moore A J and Tyrer J R 1990 An electronic speckle pattern interferometer for complete in-plane displacement measurement *Meas. Sci. Technol.* **1** 1024-30
[25] Løkberg O J and Høgmoen K 1976 vibration phase mapping using electronic speckle pattern interferometry *Appl. Opt.* **15** (11) 2701-04
[26] Huang J-R, Ford H D and Tatam R P 1996 Heterodyning of speckle shearing interferometers using laser diode wavelength modulation *Meas. Sci. Technol.* **7** 1721-7
[27] Atcha H and Tatam R P 1994 Heterodyning of Fibre Optic Electronic Speckle Pattern Interferometers using Laser Diode Wavelength Modulation *Meas. Sci. Technol.(Special Issue: Optical Techniques in Measurement)* **5** 704-9
[28] Creath K 1987 Step height measurement using two-wavelength phase-shifting interferometry *Appl. Opt.* **26** (14) 2810-6
[29] Hariharan P and Roy M 1995 White-light phase-stepping interferometry: measurement of the fractional interference order *J. Mod. Opt.* **42** 2357-60
[30] Malacara D 1992 Phase-shifting interferometers *Optical Shop Testing* (New York: Wiley) 501-98
[31] Grattan K T V and Meggitt B T 1999 *Optical Fiber Sensor Technology* vol 3 (Dordrecht: Kluwer Academic) 243-4
[32] Zissis G J and Larocca A J 1978 Optical Radiators and Sources *Handbook of Optics* (New York: McGraw Hill Book Company) 3.1-3.40
[33] Yurek A M and *Dandridge* A 1988 Optical Sources *Optical Fiber Sensors: principles and components* (Boston and London: Artech House)
[34] Gerges A S, Newson T P and Jackson D A 1990 Coherence tuned fiber optic sensing systems with self-initialization, based on a multimode laser diode *Appl. Opt.* **29** (30) 4473-80
[35] Ho T K, Fujimoto J G, de Matos C J S, Popov S V, Broeng J, Gapontsev V P and Taylor J R 2005 All-fiber, cw, Raman continuum light source for ultrahigh resolution optical coherence tomography *Proc. Fiber Lasers II: Technology, Systems and Applications, Laser 2005, Photonics West (San Jose, USA, 22-27 January 2005)* SPIE 5709-34
[36] Wyant J C 1971 Testing aspherics using two-wavelength holography *Appl. Opt.* **10** 2113-8
[37] Wang D N, Ning Y N, Grattan K T V, Palmer A W and Weir K The optimized wavelength combinations of two broad-band sources for white light interferometry *J. Lightwave Technol.* **12** 909-15
[38] Wang C, Xiao H, Hong H and Ye S Pulsed laser diode optical fiber interferometer absolute distance measurement *Proc. Soc.Photo-Optical Instrumentation Engineers: Fiber optic and laser sensors XIV (Denver, USA, 1996)* SPIE 2839 350-2

[39] Peterman K and Arnold G 1982 Noise and distortion characteristics of semiconductor lasers in optical fiber communication systems *IEEE J. Quantum Elect.* **QE-18** 543-55
[40] Moore A J and Tyrer J R 1990 An electronic speckle patter interferometer for complete in-plane displacement measurement *Meas. Sc. Technol.* **1** 1024-30
[41] Olszak A and Tatam R P 1997 The calibration of the path-length imbablance in optical fibre ESPI systems employing source wavelength modulation *Meas. Sc. Technol.* **8** 759-63
[42] Hariharan P, Oreb B F and Eiju T 1987 Digital phase-shifting interferometry: a simple error-compensating phase calculation *Appl. Opt.* **26** (13) 2504-6
[43] Fales G 2003 *Sensors Magazine Online* October issue
[44] Valera J D, Doval A F and Jones J D C 1993 Combined fibre-optic laser velocimeter and electronic speckle pattern interferometer with a common reference beam *Meas. Sci. Technol.* **4** 578-82
[45] Charters R B, Staines S E and Tatam R P 1994 In-line fiber-optic components using Langmuir-Blodgett films *Opt. Lett.* **19** 2036-8
[46]Jackson D A, Priest R, Dandridge A and Tveten A B 1980 Elimination of drift in a single-mode optical fiber interferometer using a piezoelectrically stretched coiled fiber *Appl. Opt.* **19** 2926–9